ELECTROMAGNETIC PHENOMENA IN AN ELECTRIC SUBMERGED ARC FURNACE

KARALIS Konstantinos, KARKALOS Nikos, ANTIPAS G.S.E, XENIDIS Anthimos

School of Mining Engineering and Metallurgy, National Technical University of Athens, Zografou Campus, Athens, Greece, EU, kkaral@metal.ntua.gr

Abstract

A three-dimensional mathematical model has been developed in order to describe the electromagnetic phenomena in an Electric submerged Arc Furnace (EAF). From the electromagnetics differential equations solution, the current density, Lorentz force and Joule heating was investigated in connection with the slag's electrical conductivity values. A first approach towards the determination of the slag's electrical conductivity was attempted using the 3D computational model in time dependent conditions associated with electrical potential and current measurements taken from industrial installations. It was determined that the electrical conductivity of slag was 30 S/m.

Keywords: Submerged-arc electric furnace, Söderberg electrodes, magneto-hydrodynamics, Joule heating, CFD

1. INTRODUCTION

Ferronickel is produced in submerged-arc electric furnaces (EAF), by chemical reduction of nickel laterite ores [1-3]. In Greece laterites are treated by LARCO S.A. following roasting reduction in four rotary kilns and smelting reduction in five EAFs. In **Fig. 1(a)**, the air, slag and ferronickel layer are displayed as well as the firebricks layers, which contribute to the system's thermal insulation. The ferronickel production inside the EAFs is achieved through two stages; the first stage consists of the nickel laterite ores melting and the second stage is the chemical reduction of the melted iron and nickel oxides with the carbon constituents. The necessary energy required for the aforementioned two stages inside the EAF, is introduced through three self-baked carbon electrodes (Söderberg electrodes) which are partially submerged into the slag (0.4-0.7 m). The electric current which passes through the slag and ferronickel transforms into heat according to the Joule heat phenomenon. Consequently the higher velocity inside the slag layer (corresponding to higher temperature fluctuations and lower viscosity values) results in lower ferronickel losses in slag. The main stirring phenomenon which has been reported in the literature owing to thermal buoyancy effects, contributions of electromagnetic Lorentz-type forces and momentum exchange between carbon monoxide bubbles, which are continuously released from the reduction with the oxygen of the Söderberg electrodes, and the metal bath [4-12]. However, Karalis et. all (2015) have reported that the stirring effect through the Lorentz forces and carbon monoxide bubbles released from the Söderberg electrodes can be neglected [13].

The main parameter, which is considered crucial for the EAF operation and efficiency, is the electrical conductivity of the slag. Unfortunately, the experimental determination of its value is very difficult; consequently assumptions have to be made. The overall electric resistance per pair of electrodes, can be expressed as a function of slag electrical conductivity, σ, and furnace geometric factor, f_g

$$R = \frac{f_g}{\sigma}. \tag{1}$$

Due to the fact that the electrical resistance of the graphite electrodes and ferronickel is much smaller than that of slag (25.000 S/m and approx. 750.000 S/m respectively instead of 1-100 S/m) their contribution in the total resistance can be neglected [14]. The total resistance in the case of the LARCO's EAF is 0.0074 Ω and the geometric factor ranges between 0.2-0.7 m^{-1} mainly according to the electrodes immersion depth and slags thickness.

The three electrodes are connected to operate under delta resistance configuration. The three electrodes are loaded with electric potential equal in magnitude with a phase sift of 120º. In the current study, transient conditions have been applied. The alternating current (AC) in the three electrodes is described as

$$V = V_0 \sin(\omega t) \tag{2}$$

$$V = V_0 \sin(\omega t + 120\pi/180) \tag{3}$$

$$V = V_0 \sin(\omega t + 240\pi/180), \tag{4}$$

where V_0 is the direct current (DC) component of the applied field equal to 380V, ω is the angular frequency (ω=2πf), f is the frequency applied (equal to 5Hz) and t is the time (s).

The most important assumption made during the above modeling, was the decrease of the actual current frequency from 50Hz to 5Hz. This is done in order to be able to use higher time-steps in the computational procedure.

2.   MODEL FORMULATION

Fig. 1 (a) and **(b)** illustrates the geometry of the electrodes and EAF studied. The electrodes immersion depth defined 0.6 m. Three electrodes used equally spaced from the central furnace axis with an angle between each other of 120°.
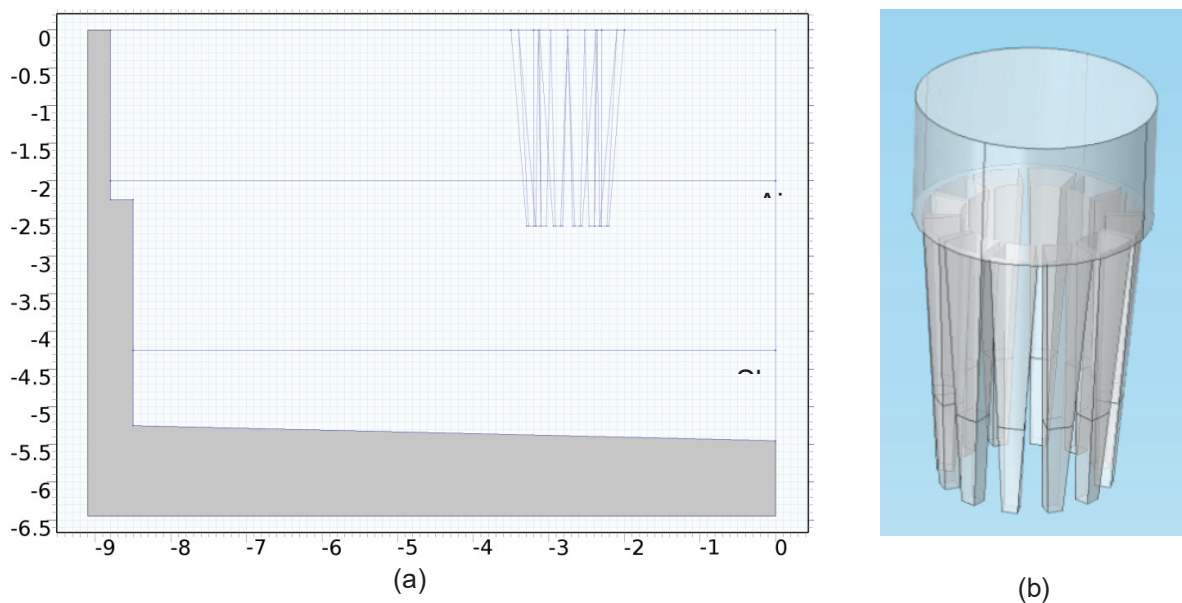
Fig. 1 (a) EAF cut plane geometry (b) Electrode geometry

Governing equations

Three electromagnetic phenomenon have been solved in the current model. The electric current balance is defined by the equation (5). Due to the materials resistance in the electric current heat is produced according to the equation (6) (Joule heating).

The electronic current balance is defined by the equation

$$\nabla \cdot (-\sigma_{metal} \nabla V) = 0 \tag{5}$$

$$Q = \sigma_{metal} |\nabla V|^2, \tag{6}$$

where σ_{metal} denotes the electric conductivity of the respective phase (S/m) and V the electric potential (V) [15].

Boundary conditions

In the furnace freeboard the normal gradient of the electric potential was assumed to be zero [4, 5, 11, 16]. In the bottom and sidewall firebricks of the furnace, ground potential (0 V) has been applied. In the upper electrodes surfaces an electric potential according to equations (2-4) was applied.

Materials properties

All the phases calculated (air, slag and ferronickel) have been considered as homogeneous fluid continuums. The density and viscosity of the slag layer as well as the electrical conductivity of the ferronickel layer were specified as piecewise linear functions of temperature in order to incorporate temperature variability into the models. **Table 1** shows analytically the electrical conductivity of the materials used in the simulations.

Table 1 Electrical conductivity values of the materials used in the simulations [17-25].

Properties	Slag	Ferronickel	Electrodes	Firebricks
Electrical conductivity (S/m)	10-60	10^6-330.83T	25000	0.01

Computational details

The numerical simulations were performed with the commercial CFD software COMSOL Multiphysics. Convergence has been assumed when the scaled residuals were below 10^{-6} in all runs. The thermal and electromagnetic variables were grouped and sequentially solved using COMSOL's segregated solver feature. The linear solver PARDISO has been used since it performed better in a multi-threading shared memory node [26]. The final grid consisted of 396332 free tetrahedron mesh elements with the worst element having a minimum and average element quality of 0.081 and 0.708 respectively. The element quality for the tetrahedron mesh is described from the equation,

$$q = \frac{72\sqrt{3}V}{\left(h_1^2+h_2^2+h_3^2+h_4^2+h_5^2+h_6^2\right)^{3/2}}, \tag{7}$$

where V is the volume and h_1 - h_6 are the side lengths of the tetrahedron. If q>0.1 the mesh quality should not affect the quality of the solution [27].

3. RESULTS AND DISCUSSION

A set of time-dependent numerical investigations was carried out, using COMSOL Multiphysics software in order to determine the characteristics of the electromagnetic phenomena that are present in the arc furnace, to validate the model in accordance to available experimental results and finally estimate slag electrical conductivity value. After the numerical investigations were carried out, results concerning various electromagnetic quantities, such as electric potential, current density and Joule heat are obtained and discussion about them is made.

3.1. Electric potential and current density distribution

A typical electric potential profile for electric arc furnaces is shown at **Fig. 2 (a)**. It can be seen that, at the specific time (600 s), two of the three electrodes have negative voltage and the other electrode positive. The largest portion of the metal bath has voltage values near zero voltage and only a small area around each electrode is affected by the electrode voltages. This profile is similar to profiles obtained using a 2D multiphysics model [13].

Current density is a physical quantity associated directly with the electric current. Thus, the current density results allow for useful conclusions concerning the flow of electric current to be drawn. In **Fig. 2 (b)** isosurfaces of current density magnitude in the range from 0.05 to $1.95 \cdot 10^4$ A/m within the EAF are portrayed. It is evident

that higher values of current density appear in the vicinity of the three electrodes, within the slag layer. However, there exists also a region within the ferronickel layer, where high values of current density are observed. Consequently, large portions of electric current flow through these regions and induce higher Lorentz forces which contribute to a more intense bath stirring effect. As for the Lorentz forces developed in the bath, it can be seen from **Table 2** that they increase with an increase of electrical conductivity. Additionally, a vector diagram on a horizontal section of the EAF (upper slag surface) is presented in **Fig. 3(a)**, with a view to determine the electric current pathways. The electric current is shown to flow from the electrode with positive voltage towards the two electrodes with negative voltage, thus following the conventional current direction. Moreover, due to the electric potential difference between the electrodes and the sidewalls, there is a smaller portion of current flowing towards this direction. Regarding the electric density dependence of the slag electric conductivity, it can be seen in **Table 2**, that an increase of the electric conductivity values leads to a direct increase of the electric density values and subsequently, larger quantities of current flow through the metal bath.
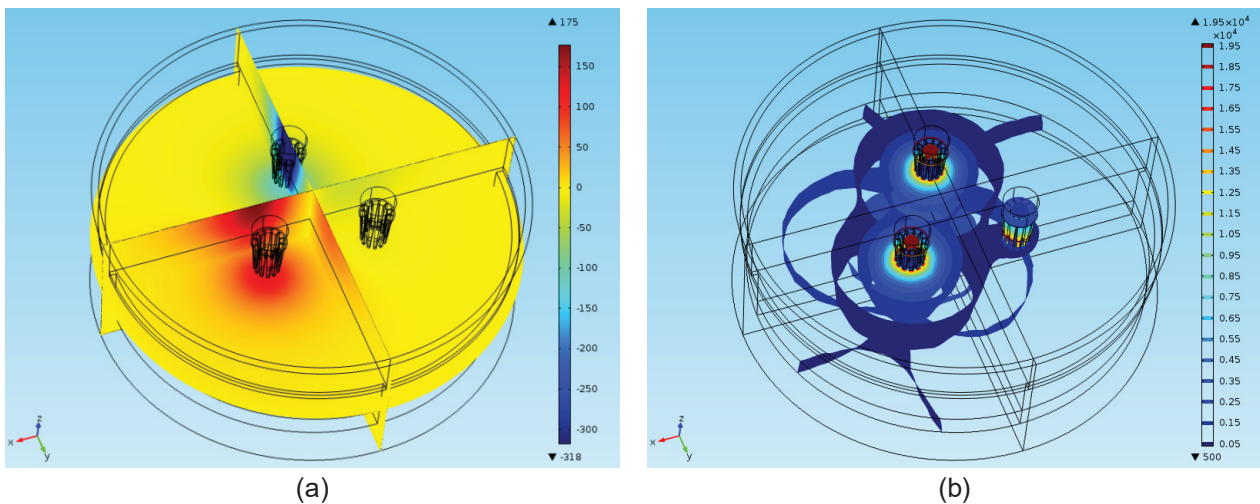
Fig. 2 (a) Electrical potential distribution in the EAF (b) current density isosurfaces

3.2. Joule heat distribution

It can be observed, from **Figs. 2(b)** and **3(b)**, that the Joule heat distribution is similar to the current density distribution because the two quantities are directly related. The study of the Joule heat distribution is important as high values of Joule heat give rise to higher temperatures and subsequently favor the melting phenomenon in certain regions of the bath. At the same time, higher temperatures lead to greater density differences within the metal bath and cause a more intense thermal buoyancy phenomenon. As it can be seen in **Fig. 3 (b)**, higher values of Joule heat appear in the vicinity of each electrode and fade quickly towards the sidewalls and the bottom of the furnace. From **Fig. 3 (b)**, it is evident that the region of high Joule heat values depends on the voltage of each electrode. Subsequently, it can be assumed that the melting phenomenon is facilitated in these regions and as the process progresses, melting advances slowly towards the entire volume of the furnace. Moreover, it can be seen that Joule heat values are significantly greater in the slag layer; it is justified due to the considerable difference between the electric conductivity values of slag and ferronickel, which are presented in **Table 1**. Furthermore, in **Table 2**, it can be observed that higher values of electric conductivity lead to higher values of Joule heat and their relationship is proportional.

(a)   (b)
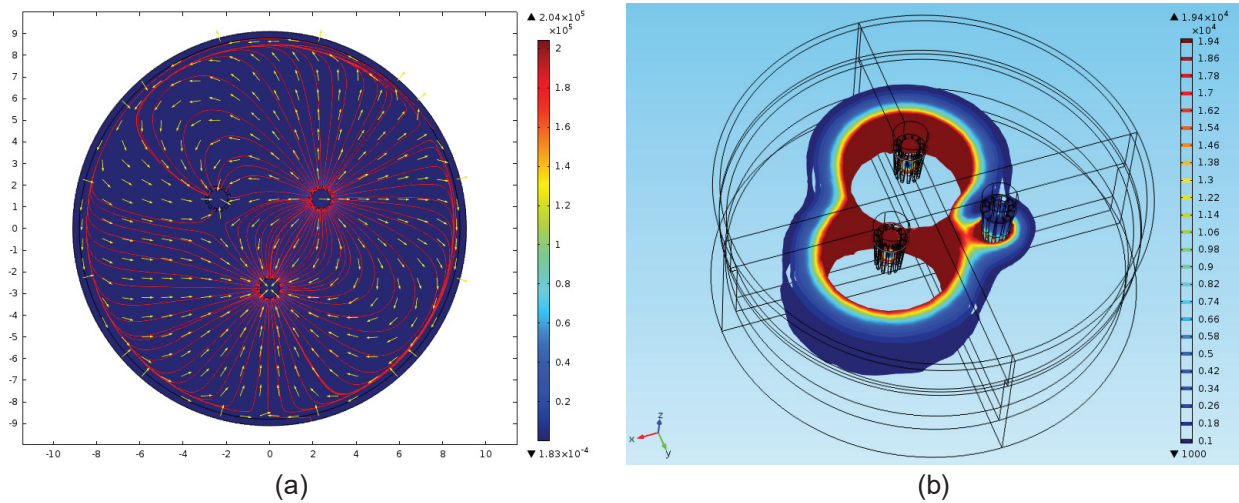
Fig. 3 (a) Current density vector plot at a horizontal section of the EAF (b) Joule heat isosurfaces in the EAF

3.3. Estimation of slag electric conductivity

After the main electromagnetic phenomena within the EAF are identified, the parametric study with varying slag electrical conductivity values was carried out as a self-consistent method to determine the exact value of slag electrical conductivity. In order to determine this value, the amount of current introduced to the slag and ferronickel layer is being calculated by integrating the electric current density values on the outer immersed electrodes surfaces. The more appropriate electric conductivity value is found when the computed current value matches industrial data; namely 68-72kA for a maximum voltage of 380V. The results of this process are displayed in **Table 2** where it can be seen that the appropriate slag's electrical conductivity values is 30 S/m. A more detailed study, involving a more complex model and focusing within this range of values, should be carried out with a view to determine more accurately the correct electric conductivity value of the specific slag.

Table 2 Values of electromagnetic quantities for cases with various slag electrical conductivity values and immersion depth of 0.6m

Slags Electrical Conductivity (S/m)	Electrodes Current (A)	Slag region average values		
		Current Density (A/m^2)	Lorentz Force (N/m^3)	Joule Heat (W/m^3)
10	25742.03	197.00	0.064	22012.16
30	75328.35	580.74	0.554	63516.80
60	154448.23	1140.53	2.093	120033.60

4. CONCLUSIONS

In this paper, a 3D time-dependent mutliphysics computational model of an EAF was created in order to investigate the electromagnetic phenomena within the EAF and the effect of slag electrical conductivity in them. Several important conclusions were drawn from these investigations:

- The electric potential, electric current density and Joule heat distributions were computed and their characteristics during a typical ferronickel smelting process were identified. It is also observed that higher values of slag electric conductivity lead to higher values of current density and Joule heat.

- The magnitude of Lorentz forces for the specific smelting process was calculated using a fully coupled electromagnetic model. It was found that the Lorentz forces increases considerably within the electrical

conductivity range 10-30 S/m. The magnitude of these forces needs to be compared with the contribution of other phenomena resulting in the bath stirring such as thermal buoyancy, with view to determine the main stirring phenomenon, a fundamental but not yet clearly resolved issue in multiphysics analysis of EAF.

- Furthermore, the parametric analysis served as a self-consistent process in order to determine the exact value of slag conductivity that matches the experimental data. The analysis revealed that the value of electrical conductivity is 30 S/m. Therefore, further investigation and experimental validation is required in order to obtain a more precise estimation of slag electrical conductivity value.

ACKNOWLEDGEMENTS

REFERENCES

[1]   Karalis, K., et al., Experimentally constrained atomic order probing of a Si-Al composite glass. Philosophical Magazine, 2014: p. 1-9.

[2]   Antipas, G.S.E., et al., Atomic order and cluster energetics of a 17 w.t.% Si-based glass versus the liquid phase. Journal of Physics: Condensed Matter, 2013. **25**: p. 1-7.

[3]   Antipas, G.S.E., et al., A containerless study of short-range order in high-temperature Fe-Si-Al-Ca-Mg-Cr-Cu-Ni oxide systems. Journal of Molecular Structure, 2012. **1019**(0): p. 151-158.

[4]   Bezuidenhout, J., J. Eksteen, and S. BRADSAW, Computational fluid dynamic modelling of a three-phase electric smelting furnace in the platinum smelting process. dimensions, 2006. **2**: p. 16.

[5]   Bezuidenhout, J., J. Eksteen, and S. Bradshaw, Computational fluid dynamic modelling of an electric furnace used in the smelting of PGM containing concentrates. Minerals Engineering, 2009. **22**(11): p. 995-1006.

[6]   Brückmann, G., G. Sick, and K. Schwerdtfeger, Slag movement in ESR of steel. Metallurgical and Materials Transactions B, 1983. **14**(4): p. 761-764.

[7]   Choudhary, M. and J. Szekely, The modeling of pool profiles, temperature profiles and velocity fields in ESR systems. Metallurgical Transactions B, 1980. **11**(3): p. 439-453.

[8]   Jardy, A., D. Ablitzer, and S. Jorget. Modelling of slag behaviour in a non-ferrous smelting electric furnace. in The Reinhardt Schuhmann International Symposium on Innovative Technology and Reactor Design in Extraction Metallurgy. 1986.

[9]   Jardy, A., D. Ablitzer, and J. Wadier, Magnetohydronamic and thermal behavior of electroslag remelting slags. Metallurgical Transactions B, 1991. **22**(1): p. 111-120.

[10] Sheng, Y., G. Irons, and D. Tisdale, Transport phenomena in electric smelting of nickel matte: Part II. Mathematical modeling. Metallurgical and materials transactions B, 1998. **29**(1): p. 85-94.

[11] Xia, J. and T. Ahokainen, Numerical modelling of slag flows in an electric furnace. Scandinavian journal of metallurgy, 2004. **33**(4): p. 220-228.

[12] Choudhary, M. and J. Szekely, The effect of temperature dependent electrical conductivity on flow and temperature fields in slags in ESR systems. Metallurgical and materials transactions B, 1981. **12**(2): p. 418-421.

[13] Karalis, K., et al., Sensitive analysis-driven CFD resolution of an industrial submerged-arc electric furnace under review, 2015.

[14] Jiao, Q. and N. Themelis, Correlation of geometric factor for slag resistance electric furnaces. Metallurgical Transactions B, 1991. **22**(2): p. 183-192.

[15] Multiphysics, C., 4.3 User's Guide. 2012, Comsol.

[16]   Ritchie, S. and J. Eksteen, Investigating the effect of slag bath conditions on the existence of multiphase emulsion zones in PGM smelting furnaces using computation fluid dynamics. Minerals Engineering, 2011. **24**(7): p. 661-675.

[17]   Atlas, S., Verlag Stahleisen GmbH, Düsseldorf. 1995, ISBN 3-514-00457-9.

[18]   Ho, C.Y., et al., Electrical resistivity of ten selected binary alloy systems. Journal of physical and chemical reference data, 1983. **12**(2): p. 183-322.

[19]   Mills, K., L. Yuan, and R. Jones, Estimating the physical properties of slags. Journal of the Southern African Institute of Mining and Metallurgy, 2011. **111**(10): p. 649-658.

[20]   Secco, R., Viscosity of the outer core. AGU reference shelf, 1995. **2**: p. 218-226.

[21]   Woolger, C., Invar nickel-iron alloy: 100 years on. Materials world, 1996. **4**(6): p. 332-333.

[22]   Mills, K., The estimation of slag properties. South African Pyrometallurgy, 2011.

[23]   Kekkonen, M., H. Oghbasilasie, and S. Louhenkilpi, Viscosity models for molten slags. 2012.

[24]   Quested, P., et al., Measurement and estimation of thermophysical properties of nickel based superalloys. Materials Science and Technology, 2009. **25**(2): p. 154-162.

[25]   Faraji, M. and H. El Qarnia, Numerical study of melting in an enclosure with discrete protruding heat sources. Applied Mathematical Modelling, 2010. **34**(5): p. 1258-1275.

[26]   Petra, N. and K.G. Matthias. Parallel performance studies for COMSOL Multiphysics using scripting and batch processing. in Proceedings of the COMSOL Conference. 2009.

[27]   COMSOL-Multiphysics, Reference Guide. 2008.